ELSEVIER

Composites Science and Technology 61 (2001) 205–220

COMPOSITES SCIENCE AND TECHNOLOGY

www.elsevier.com/locate/compscitech

The effects of glass-fiber sizings on the strength and energy absorption of the fiber/matrix interphase under high loading rates

M. Tanoglu [a,1], S.H. McKnight [b], G.R. Palmese [a], J.W. Gillespie Jr. [a,c,*]

[a] *Department of Materials Science and Engineering, Center for Composite Materials, University of Delaware, 201 Composites Manufacturing Laboratory, Newark 19716-3144, DE 19716, USA*

[b] *Army Research Laboratory, Aberdeen Proving Ground, MD 21005, USA*

[c] *Department of Civil and Environmental Engineering, Center for Composites, University of Delaware, 201 Composites Manufacturing Laboratory, Newark, 19716-3144, DE 19716, USA*

Received 8 February 2000; received in revised form 20 July 2000; accepted 15 August 2000

Abstract

The interphases of various sized E-glass-fiber/epoxy-amine systems were tested at displacement rates in the range 230–2450 μm/s by a new experimental technique (dynamic micro-debonding technique). By this method, the rate-dependent interphase properties, apparent shear strength and absorbed energies due to debonding and frictional sliding, were quantified. The systems include unsized, epoxy-amine compatible, and epoxy-amine *in*compatible glass fibers. The high displacement rates that induce high-strain-rate interphase loading were obtained by using the rapid expansion capability of piezoelectric actuators (PZT). The results of dynamic micro-debonding experiments showed that the values of interphase strength and specific absorbed energies varied in a manner that is dependent on the sizing and exhibited significant sensitivity to loading rates. The unsized fibers exhibit greater frictional sliding energies that could provide better ballistic resistance, while the compatible sized fibers show higher strength values that improve the structural integrity of the polymeric composites. In addition, significantly higher amounts of energy are absorbed within the frictional sliding regime compared to debonding. By using the experimental data obtained, a case study was performed to reveal the importance of the interphase related micro damage modes on energy absorption (and therefore ballistic performance) of glass/epoxy composite armor.

Keywords: A. Coupling agents; A. Polymer-matrix composites (PMCs); B. Interphase: B. Fiber/matrix bond; B. Impact behavior

1. Introduction

Composite materials are playing a key role in the development of lightweight integral armor for military vehicles such as tanks or armored personnel carriers. For future applications, revolutionary approaches are required to significantly reduce (up to 50%) the mass of these systems and improve their mobility and transportability without sacrificing survivability or maintainability. Recent advances in lightweight armor include the development of composite/ceramic integral armor systems as represented in Fig. 1. The lightweight integral armor design includes multiple layers of glass fiber reinforced-polymeric composite to meet the structural and ballistic requirements. Sized glass fibers are being used with epoxy, vinyl-ester and polyester resin systems for these applications.

Interphases in composites form in the vicinity of fiber surfaces and may exhibit significantly different material characteristics than the bulk resin properties [1–6]. The properties of the interphase and degree of adhesion between the fiber and matrix govern load transfer between the composite constituents. Also, the properties of the interphase are critical to global composite performance such as strength, toughness, durability and impact/ballistic resistance [6–14]. An optimum balance of structural, ballistic/impact and durability performance from the composite armor can be achieved by tailoring the fiber/matrix interphase.

In addition to the composite performance, it has been recognized in recent years that the properties of the interphase may affect the energy absorption in the composites used for lightweight armor applications. The

* Corresponding author.

[1] Current address: Izmir Institute of Technology, Urla, Izmir, Turkey.

E-mail address: gillespie@ccm.udel.edu (M. Tanoglu).

0266-3538/01/$ - see front matter
PII: S0266-3538(00)00195-0

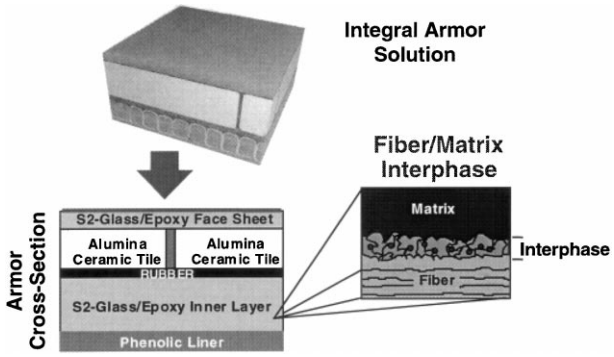

Fig. 1. Representative integral armor design. Integral armor includes multiple layers of glass-fiber reinforced epoxy composites.

mechanisms through which energy is absorbed during dynamic loading are critical to the ballistic or impact resistance of fiber-reinforced composites. The damage mechanisms include interphase-related micro-mechanisms as well as macro-mechanisms. It has been shown in the literature that micro-mechanisms such as fiber/matrix debonding or frictional fiber sliding are more important energy-absorbing mechanisms than macro-mechanisms such as delamination or matrix cracking under certain conditions [15–17]. The relative contribution of each energy-absorbing mechanism depends on the properties of the constituents (fiber, matrix and interface/interphase) as well as the mode and rate of loading [15,18]. It is necessary to know the strain rate dependent behavior of the composite constituents (fiber, matrix and interphase) to gain insight into the design of new materials that undergo loading (e.g. impact, ballistic and explosive). Techniques to directly characterize the mechanical properties of the interphase exist but have been limited to quasi-static loading.

Recently, a new experimental technique (dynamic micro-debonding technique) was developed to directly characterize the fiber/matrix interphase properties under various loading rates [19]. For this technique, a new apparatus called the dynamic interphase-loading apparatus (DILA) was designed utilizing the fast expansion capability of piezoelectric actuators. This method enables one to quantify the interphase strength and the energy absorption due to debonding and frictional sliding over a wide range of loading rate. The loading rate achieved using DILA is about three orders of magnitude (up to about 3000 μm/s) faster than the rates reported in the literature using traditional methods.

Several researchers [6–8] studied various glass fiber sizings to understand their effects on the interphase formation and composite mechanical behavior. These studies revealed that fiber sizings play a major role in the strength, impact/ballistic and environmental durability of glass-fiber reinforced composites. Sizings coated on glass fibers consist of mixtures of film formers, surfactants, silane coupling agents and other processing aids. The sizing mixture is applied from an aqueous emulsion during the manufacture of glass fibers. During the drying process of glass fiber sizings, a siloxane layer forms on the fiber surface due to the condensation and cross-linking reactions of the silane coupling agent. The siloxane is chemically bonded to the surface and strengthens the bond between the inorganic glass and organic resin phase. It has been shown that the extractable portion of the sizing dissolves into the resin during the curing process [6,19]. On the other hand, a portion of the sizing remains bound to the surface that affects the chemistry and properties of the interphase [19]. The weight fraction and the chemical composition of the bound sizing layer on epoxy-amine compatible and epoxy-amine *in*compatible glass fibers have been identified previously [19,20]. Furthermore, a new methodology was developed to indirectly evaluate the properties of the interphase that may form by the presence of bound (chemically or physically attached) glass fiber sizings. Model interphase compounds were made to replicate the composition and network structure of the actual interphase [19,20]. The investigation of the rate-dependent behavior of model interphase materials using dynamic mechanical analysis (DMA) showed that the values of storage modulus increase with the loading rate [20].

The aim of the present work is to investigate the effects of various glass fiber sizings and the loading rate on the mechanical response of the glass/epoxy interphase using the dynamic micro-debonding technique. The glass fibers examined include unsized, epoxy-amine compatible and epoxy-amine *in*compatible sized fibers. The test technique and the data reduction scheme used to quantify the strength and specific absorbed energies due to debonding and frictional sliding are summarized. Test results obtained using DILA from the interphase of composite made from these sized fibers and epoxy-amine resin are presented. Finally, a case study is presented on a typical glass/epoxy composite subjected to ballistic impact to determine the significance of the interphase-related micro damage modes in absorbing the impact energy.

2. Experimental

2.1. Materials and specimen preparation

E-glass fiber — unsized (159A), epoxy-amine compatible sized (159E), and epoxy-amine *in*compatible sized (159I) custom made for this work by Owens Corning Corporation — were used in this investigation. The sizing mixture for the sized fibers contains three components: epoxy film former, surfactant, and silane coupling agent. The film former was diglycidyl ether of bisphenol-A (DGEBA) with the average molecular weight of

515 g/mol. The surfactant was a triblock ethylene oxide and propylene oxide copolymer. The silane coupling agent was glycidoxy propyl trimethoxy silane and methacryloxy propyl trimethoxy silane for epoxy-amine compatible (159E) and epoxy-amine *in*compatible (159I) fibers, respectively. The sizing components and their weight percentage are shown in Table 1. The compatibility and incompatibility of the sizing is often defined based on the reactivity of the coupling agent with the resin system used. Namely, 159E sizing is compatible with epoxy-amine resin due to the epoxide group on the organic tail of the silane coupling agent that can react with amine in the matrix resin. Comparison of compatible versus *in*compatible sizing allows us to isolate the effect of chemical bonding between the interphase and the matrix on the interphase strength and energy absorption. In addition, the study of unsized fiber provides insight into the effect of sizing and the chemical bonding on interphase properties.

The matrix material was an epoxy/amine system comprised of DGEBA (Shell Epon-828), and a bis (*p*-amino cyclohexyl) methane (Air Products, Amicure PACM-20). The average molecular weight of Epon-828 is 370 g/mol. Epon-828 and PACM-20 were mixed in a 100/28 parts-by-weight stoichiometric ratio for all samples made in this study. The mechanical properties of the epoxy-amine matrix and the glass fibers are listed in Table 2.

Table 1
E-glass fibers used in this investigation. The sizing components and their weight percentage are also shown

Fiber designation	159A fiber	159E fiber	159I fiber
Sizing	Unsized	Epoxy-amine compatible sized	Epoxy-amine *in*compatible sized
Sizing system			
Film former (wt.%)	–	Epoxy (67)	Epoxy (67)
Silane (wt.%)	–	Glycidoxy (15)	Methacryloxy (15)
Surfactant (wt.%)	–	PEO-co-PO* (18)[a]	PEO-co-PO* (18)[a]

[a] PEO-co-PO*: Poly (ethylene oxide-co-propylene oxide).

Table 2
Mechanical properties of the epoxy-amine matrix and the E-glass fibers

	Matrix (Epon-828/PACM-20)[a]	Fiber (E-glass)
Young's modulus, E (GPa)	2.5	72
Shear modulus, G (GPa)	0.925	28.57
Poisson ratio, ν	0.35	0.26
Density, ρ (g/cm^3)	1.15	2.54
Fiber diameter, d (μm)	–	21±3

[a] At stoichiometric composition, cured at 80°C for 2 h, post-cured at 150°C for 2 h.

Test specimens were prepared by placing a bundle of glass fibers in silicone rubber and pouring degassed epoxy/amine resin mixture over the fibers. The specimens were cured at 80°C for 2 h and post-cured at 150°C for another 2 h. Following post-cure, the specimens were sectioned perpendicular to the fiber direction using a diamond blade. The sectioned specimens were then ground and polished to a 0.1-μm finish using a variety (6, 3, 1 and 0.1-μm) of diamond pastes. The polishing process was continued until the specimen thickness (h) was reduced to approximately 100 μm. The polished specimens were inspected using optical microscopy to screen samples that were damaged during the polishing process. The fiber diameter was measured using optical microscopy, and the specimen thickness was measured using a micrometer.

2.2. Experimental techniques

In this work, the dynamic micro-debonding technique was used to directly characterize the fiber/matrix interphase properties under various loading rates. Table 3 summarizes the characteristics of the dynamic micro-debonding technique. A schematic of the test configuration is shown in Fig. 2. More detailed information about the technique was reported elsewhere [19,21]. In summary, a thin sample of thickness h is mounted on a steel annulus with radius r_a. A diamond tip that is attached to a piezo stack is used as a probe to load the fiber and, therefore, the interphase region. While the interphase is loaded, the force and displacement responses are monitored continuously. The displacement of the piezo is measured from the displacement sensor (sensitivity in nanometer) attached on the piezo stack. The force response of the specimen is monitored using a piezo load cell that has high frequency capacity with 0.05 N sensitivity.

During the test, once the contact is made between the diamond tip and one fiber end, the piezo is triggered to

Table 3
Summary of dynamic micro-debonding technique

Typical dimensions
Sample thickness (h): ~ 100 μm
Fiber radius (r_f): 4–25 μm
Annulus radius (r_a): 25 μm

Displacement rates
100–3000 μm/s

Measured response
Force, displacement vs. rate

Calculated interphase properties vs. rate
Strength
Energy to debonding
Energy to sliding

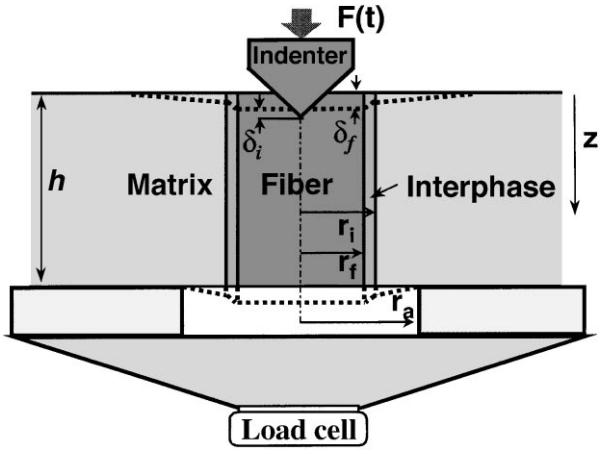

Fig. 2. Schematic of test configuration and the micro-debonding process.

impose the piezo displacement (δ_p). The piezo displacement results in displacement of the fiber relative to the matrix (δ_f). For accurate interphase property calculations, various sources of compliance must be quantified to isolate the fiber displacement. The actual displacement of the fiber (δ_f) can be determined by subtracting the indentation displacement on the fiber surface (δ_i) and apparatus (i.e. machine compliance) displacement δ_a from the displacement of the piezo actuator as follows [19]:

$$\delta_f = \delta_p - \delta_i - \delta_a \tag{1}$$

For rigid fibers such as glass (e.g. E-glass fiber, Young's modulus of 72 GPa), it is considered that δ_f is the displacement of the entire fiber instead of the displacement of the top surface of the fiber. The amount of displacement due to indentation δ_i and apparatus deformation δ_a was measured independently as a function of applied force [19,21]. For this purpose, DILA was used to perform a micro-indentation experiment on a bulk E-glass sample. Atomic force microscopy (AFM) was used to quantify the amount of residual indentation deformation on the glass samples. The values of δ_i and δ_a as a function of applied force were curve fitted, and the obtained values were subtracted from the displacement of the piezo actuator at each force level. It was assumed that the effect of the strain rate on the amount of indentation displacement is negligible. Based on these micro-indentation experiment results, the displacement of the fiber (δ_f) was determined based on Eq. (2) at a given applied force (F). Fig. 3 is an example showing the piezo displacement, indentation and machine displacement and the corrected fiber displacement as a function of force (F).

The axial displacement of the fiber causes shear deformation of the interphase region. The amount of interphase deformation depends on the relative axial displacement of the fiber and matrix adjacent to the interphase material. Once it fails, further displacement results in frictional sliding of the fiber within the matrix.

In the dynamic micro-debonding technique, thin specimens (typically 100 μm thick) were used. Numerical results of Kallas et al. [22] showed that the magnitude of bending stresses at the specimen surface depends on the ratio of sample thickness to annulus diameter in thin samples. These bending stresses may alter the mode of interfacial failure. Therefore, a sensitivity study was conducted to experimentally quantify the effects of specimen geometry on the shear strength [19]. Our experiments showed that the shear strength is independent of the specimen geometry for $h/r_a < 2.8$. For $h/r_a < 2.8$, the apparent strength increases significantly. This increase may be due to a complex interaction between flexural and shear deformations as noted by Kallas et al. [22]. Samples tested had an h/r_a ratio of approximately 4 to ensure that the experimentally measured shear strength is independent of specimen geometry. Moreover, thin samples enable actual debonding length to be measured accurately, since complete fiber/matrix debonding occurs. The strength and frictional measurements can be done using the measured debonding length. This greatly simplifies data reduction as discussed in the following section, since numerical methods are not required as in the method of Mandell et al. [23].

2.3. Data reduction scheme

The fiber displacement (δ_f) is imposed by the piezo, and the dynamic reaction force $F(T)$ is measured independently through the load cell. Using the corrected fiber displacement vs. force response from the test, the following interphase properties are calculated: the average shear strength, the specific absorbed energies due to debonding and frictional sliding.

The average shear stress can be obtained from Eq. (2), where $F(t)$ is the force applied to the end of the fiber and the area calculated at the radial distance, (r), within the interphase region:

$$\tau = \frac{F(t)}{2\pi hr} \tag{2}$$

where h is the thickness of the sample (length of the fiber). In this work, the shear strength is defined using Eq. (2) and the load measured at the debonding threshold (typically the maximum load). It has been confirmed by incremental loading of the interphase using DILA in conjunction with AFM section analysis of the specimen that the maximum load (F_u) corresponds to complete debonding [19]. The strength is calculated at the fiber surface based on Eq. (3).

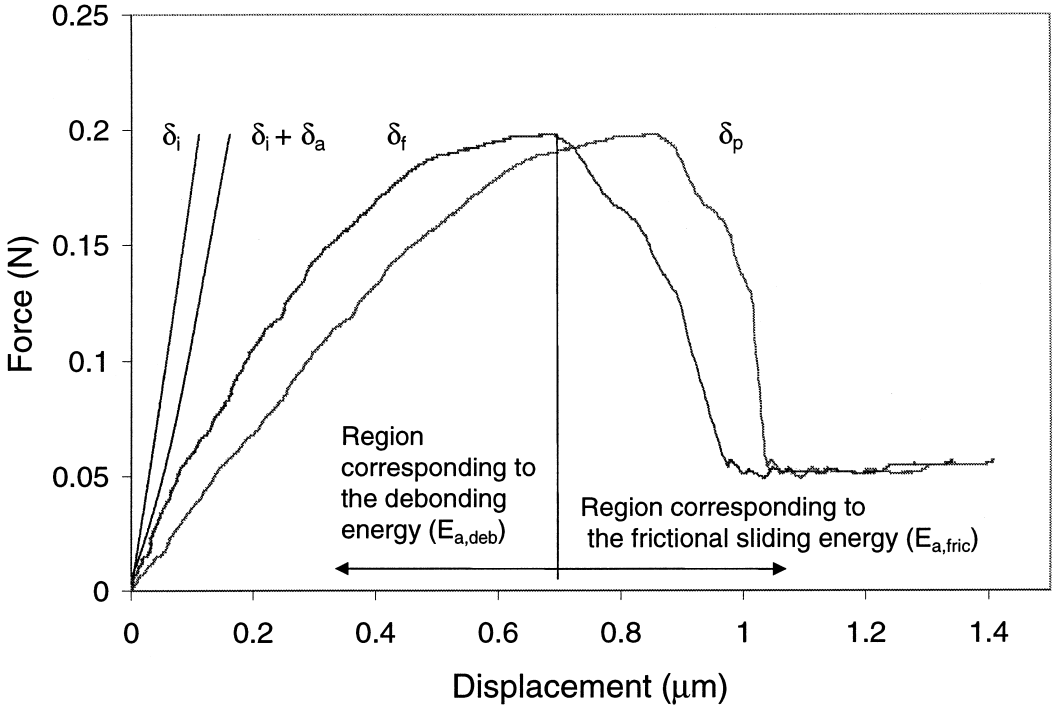

Fig. 3. The fiber displacement (δ_f), indentation displacement δ_i and deformation of the apparatus (δ_a), and the piezo displacement (δ_p) as a function of force (F). The two main energy absorbing regions corresponding to debonding and frictional sliding are also shown.

$$\tau_{max} = \frac{F_u}{2\pi h r_f} \tag{3}$$

It is assumed that inertia effects are negligible which is reasonable since the test is conducted in the millisecond regime.

The total specific absorbed energy (E_a) within the interphase during loading can be measured. The specific absorbed energy is defined as the amount of energy absorbed per unit area of loaded interphase (A). E_a was obtained based on force (F) vs. fiber displacement (δ_f) graphs using the relationship given by Eqs. (4) and (5).

$$E_a = \frac{\int_0^{\delta_{f,u}} F d\delta_f}{A} = E_{a,deb} + E_{a,fric} = \frac{\int_0^{\delta_{f,deb}} F d\delta_f}{A_{deb}} + \frac{\int_{\delta_{f,deb}}^{\delta_{f,u}} F d\delta_f}{A_{fric}} \tag{4}$$

$$A_{deb} = 2\pi r_f h \tag{5a}$$

$$A_{fric} = 2\pi r_f \left(h - \left(\delta_{f,u} - \delta_{f,deb}\right)\right) \tag{5b}$$

where $\delta_{f,deb}$ and $\delta_{f,u}$ are the displacement where debonding is complete and ultimate displacement measured, respectively. The terms A_{deb} and A_{fric} are the area of loaded interphase/interface during debonding and frictional sliding stages, respectively. Since the interfacial area during the fiber sliding process becomes smaller as the fiber is pushed out from the matrix, the reduced value of the A_{fric} is taken into account as a function of the displacement as shown in Eq. (5b). The energy absorbed due to each mechanism, i.e. debonding $(E_{a,deb})$ and frictional sliding $(E_{a,fric})$, during the loading of the interphase can be calculated from Eqs (4) and (5). This enables one to isolate energy absorbed due to debonding as well as frictional sliding as a function of loading rate.

2.4. Test procedure

The polished specimens were first mounted on an annulus with a 25-μm hole radius (r_a). The selected fibers were tested using a 60° conical tip that has an 8-μm tip radius. Piezo input signals corresponding to various displacement rates were selected and programmed into the piezo control system. To initiate a test, the selected fiber was positioned under the tip, and the loading parameters were sent to the piezo control. After triggering the system, three signals (displacement, load cell and input signals) were acquired and recorded as a function of time by the data acquisition system. After the test was complete, the specimens were inspected under optical and scanning electron microscopes to confirm the failure mode and the location of loading. The shear strength and absorbed energies due to fiber/matrix debonding and frictional sliding were calculated according to the data reduction procedures described earlier.

3. Results and discussion

The interphase of model composites made with epoxy-amine resin and various sized glass fiber systems listed in Table 1 were tested at displacement rates ($\dot{\delta}_f$) in the range of about 238 to 2410 μ/s using DILA.

3.1. Force vs. displacement response

Figs. 4–6 show typical examples of force (F) vs. displacement (δ_f) graphs obtained from the interphases of composites made with the Epon-828/PACM-20 resin and 159A (unsized), 159E (epoxy-amine compatible sized), and 159I (epoxy-amine *in*compatible sized) fibers, respectively, under various displacement rates. All of the fiber displacement values in these figures are compliance corrected displacement values. As seen in Figs. 4–6, all of these force vs. displacement curves exhibit several distinct regions. Initially, the force increases almost linearly with the displacement. In this initial part, it is expected that there is full bonding between the composite constituents, and the response of the sample is elastic. It is apparent from these figures that at some displacement values the F vs. δ_f response shows non-linearity. However, there is smooth transition from linear response to non-linear response, instead of a sharp transition or formation of an early load drop. The non-linear region extends until a maximum is reached where complete fiber/matrix debonding occurs. Once complete debonding occurs, the force drops suddenly, as seen in Figs. 4–6. At this point, further displacement of the fiber results in only frictional sliding of the totally debonded fiber within the matrix. As seen from Figs. 4–6, the initial slopes (F/δ) of the force vs. displacement curves and the maximum load levels are found to be sensitive to the loading rate and the type of fiber sizing. The measured F/δ_f response at the initial stage may be related to the shear stress/strain response of the interphase (modulus of the interphase, G_i) and it is a subject of ongoing research. In general, the initial slopes of the F/δ_f increased with the displacement rate indicating that G_i is rate sensitive. Furthermore, a less steep F/δ_f response was observed from the samples made with epoxy-amine compatible 159E and epoxy-amine *in*compatible 159I sizings compared to the unsized 159A fiber system. This indicates the formation of a more compliant interphase due to the glass fiber sizings and agrees with model studies [19,20]. Moreover, the samples made with epoxy-amine compatible 159E and epoxy-amine *in*compatible 159I sized fibers showed higher rate sensitivity compared to the unsized 159A fiber system.

The non-linearity of the F vs. δ_f response can be associated with nonlinear constitutive behavior, progressive debonding of the fiber/matrix interphase or both mechanisms. As revealed by Kallas et al. [22] and Bechel and Sottos [24,25], thin specimens exhibit significantly high tensile radial stresses at the bottom of the micro-debonding specimen. The flexural bending of the specimen and/or the residual thermal stresses may be responsible for these radial stresses [22,25]. These high tensile radial stresses may cause initiation of debonding

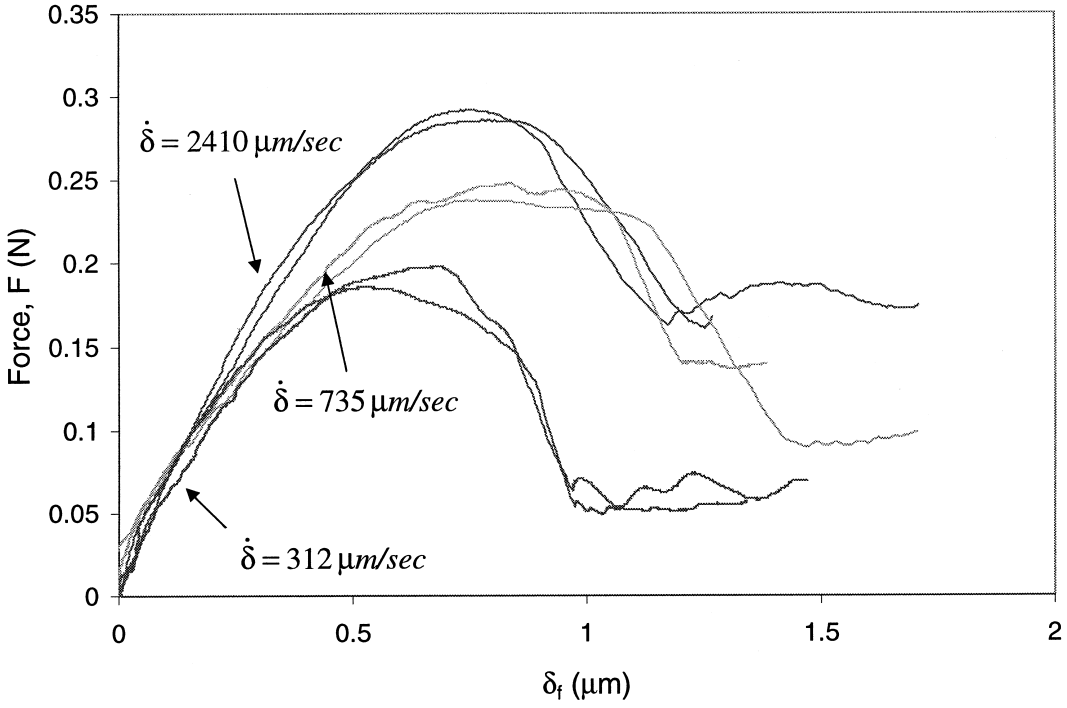

Fig. 4. Force vs. displacement graphs for 159A (water sized) E-glass-fiber/epoxy-amine interphase tested using DILA.

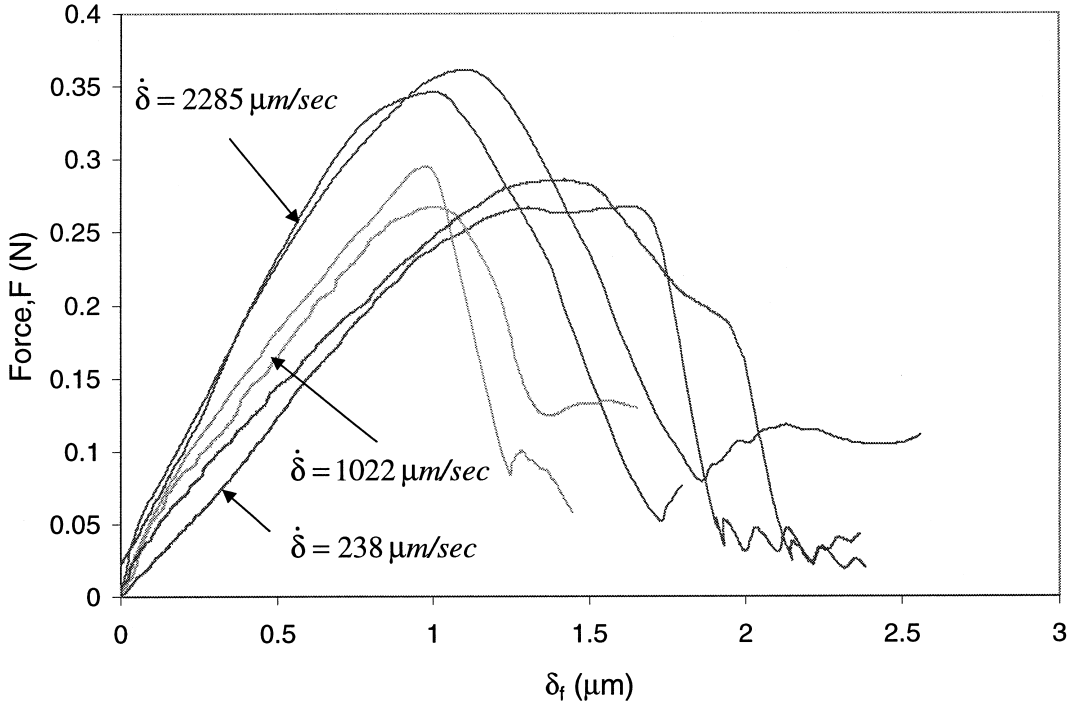

Fig. 5. Force vs. displacement graphs for 159E (epoxy-amine compatible sized) E-glass-fiber/epoxy-amine interphase tested using DILA.

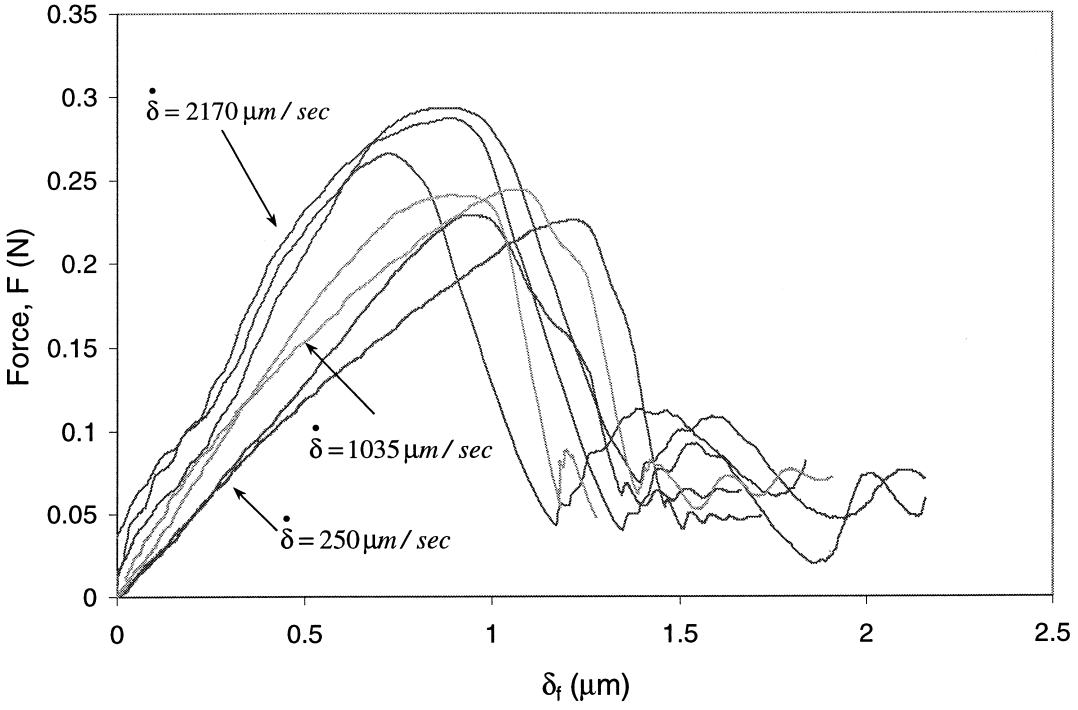

Fig. 6. Force vs. displacement graphs for 159I (epoxy-amine *in*compatible sized) E-glass-fiber/epoxy-amine interphase tested using DILA.

near the bottom surface at force levels much lower than the complete debonding force level. Once the failure initiates at the bottom, progressive debonding may occur from the bottom to the top surface. Bechel and Sottos [24] investigated the initiation and growth of the interface debonding and measured the debonding length based on the observations of the photoelastic fringe pattern development within the matrix during the pushout test. For this purpose, fiber pushout experiments on several model composites were performed in a polariscope. The result of their experiment revealed that the fiber/matrix interface may fail through progressive

debonding instead of instantaneous debonding at the maximum force level. It was also shown that the composites with a fiber-matrix modulus ratio (E_i/E_m) of greater than 4 will debond from the bottom towards the top of the specimen. Since the E/E_m is about 30 for the composite system tested in the present study, it may be expected that debonding initiates from the bottom of the samples tested here. The influence of non-linear shear behavior of the interphase on the F vs. δ_f response measured during microdebonding has not been investigated and warrants further study.

3.2. Apparent average shear strength

The apparent average shear strength values for various sized E-glass/epoxy-amine interphases were calculated using Eq. (3) for complete debonding to enable comparison with other results reported in the literature [7,23,26]. Results are presented in Fig. 7 as a function of displacement rate (at least five samples were tested for each point). The coefficient of variation shown on Fig. 7 (4.6–10.4%) is in the same range as values reported in the literature obtained from similar materials systems using quasi-static microdebonding method (as an example, 6.4–10.5% by Mandel et al. [23] and 5.5–6.8% by Drown et al. [7]). The scattering of the data could be related to possible micro-damage that develops during the polishing steps as well as the sensitivity of the calculated values to the fiber diameter and the specimen thickness measurements. Since thin samples (about 100 μm) are required, extensive polishing can induce micro damage within the specimen that may not be visible under the microscope. As revealed by Bechel and Sottos [25], initial interface debonding forms during the specimen preparation stages. It was considered that the tensile/shear stresses that develop during the cutting/polishing and the residual radial tension at the free edge contribute to initial debonding near the specimen ends.

As seen from Fig. 7, it appears that there is a linear correlation between the shear strength and the loading rates studied in this work. The average shear strength values were found to increase by about 43, 35 and 27% for unsized 159A, compatible sized 159E, and *in*compatible sized 159I fibers, respectively, for displacement rates in the range of about 230–2450 μm/s. A linear fit of the data enables the apparent quasi-static shear strengths of 37, 43 and 35 MPa for 159A, 159E, and 159I fiber systems, respectively, to be estimated. Our results are in good agreement with quasi-static data reported for similar systems that also used Eq. 3 for data reduction [26]. Determination of the interphase strength values allows for better understanding of the effects of sizing on the interphase mechanical response and the fiber/matrix adhesion. The highest strength is obtained from the compatible sized fiber (159E) and stems from the chemical bonding between the epoxy group of glycidoxy silane and the amine-curing agent of the matrix resin. The lower strength values exhibited by the *in*compatible sized fiber (159I) are due to the lack of chemical bonding between the methacryloxy silane and the matrix resin. The interphase shear strength values for the unsized (159A) fibers are lower than those of compatible sized (159E) but higher than those of *in*compatible sized (159I) fibers. This behavior is most probably due to some specific physical interactions such as polar and hydrogen bonding between the hydroxyl group of the glass fibers and the hydrogen atoms of the epoxy and/or amine of the matrix.

3.3. Specific absorbed energies due to debonding and frictional sliding

Understanding the mechanisms contributing to energy absorption is a key to tailoring the interphase to obtain the desired ballistic performance from the composite. The specific absorbed energy (E_a) within the interphase due to debonding and frictional sliding was measured using DILA based on Eqs. (4) and (5). Note that energies are calculated from the area under the force vs. displacement graphs and normalized by the shear area defined by Eq. (5). Fig. 3 is a typical example of the force vs. displacement graph showing the two main regions corresponding to debonding and frictional sliding energies.

In the first region, the energy is absorbed due to interphase debonding processes. As discussed earlier, debonding may initiate and grow progressively prior to complete debonding at the maximum force level. Consequently, the debonding energy may have a contribution from frictional sliding from the partially debonded portion of the fiber. For simplicity, no attempt is made to separate out the relative contribution in the first region (i.e. $E_{a,deb}$).

In the second region, the main energy-absorbing mechanism is frictional sliding between the completely debonded surfaces. The frictional force was defined as the secondary plateau, which is rate dependent as shown in Figs. 4–6. The energy absorbed due to frictional forces is a continuous function of displacement and strongly affected by displacement rate. Test results show that the specific energy absorbed due to frictional sliding is significantly higher than the energy absorbed due to debonding.

The average specific absorbed energies due to fiber/matrix debonding and frictional sliding as a function of displacement rate for various sized glass-fiber/epoxy-amine interphases are plotted in Figs. 8 and 9, respectively. As seen from these figures the fiber/matrix frictional sliding energies (0.8 to 2.8 kJ/m^2 in the range of 238–2410 μm/s) were significantly higher than the debonding energies (0.027–0.064 kJ/m^2 in the range of 312–2285

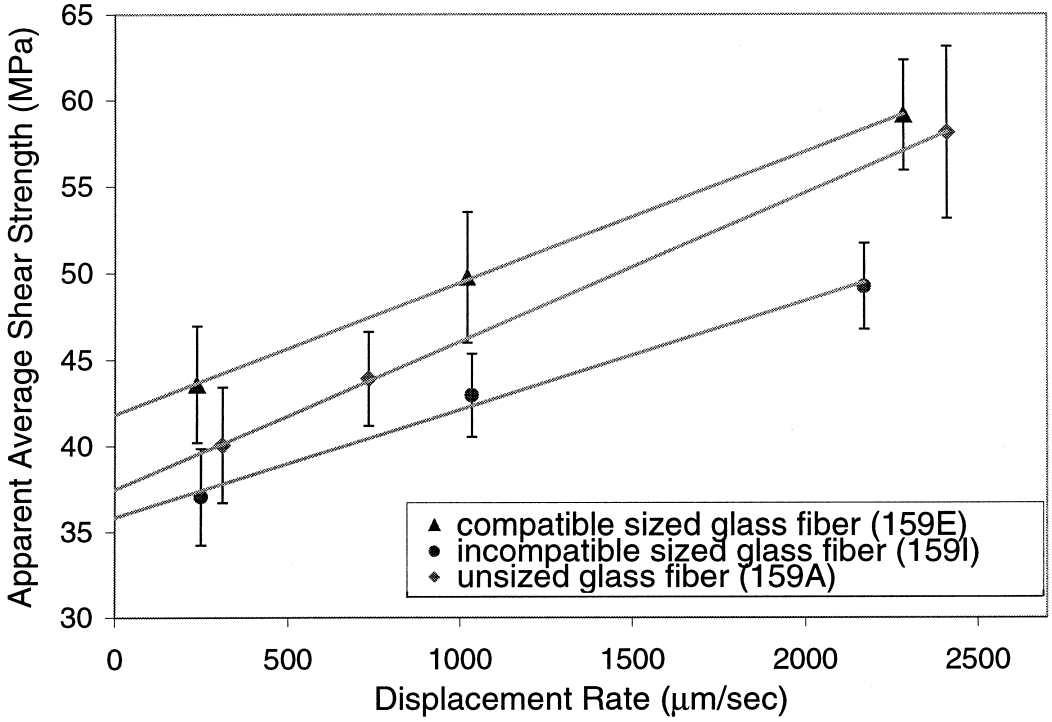

Fig. 7. Average shear strength as a function of displacement rate for various sized E-glass-fiber/epoxy-amine interphases.

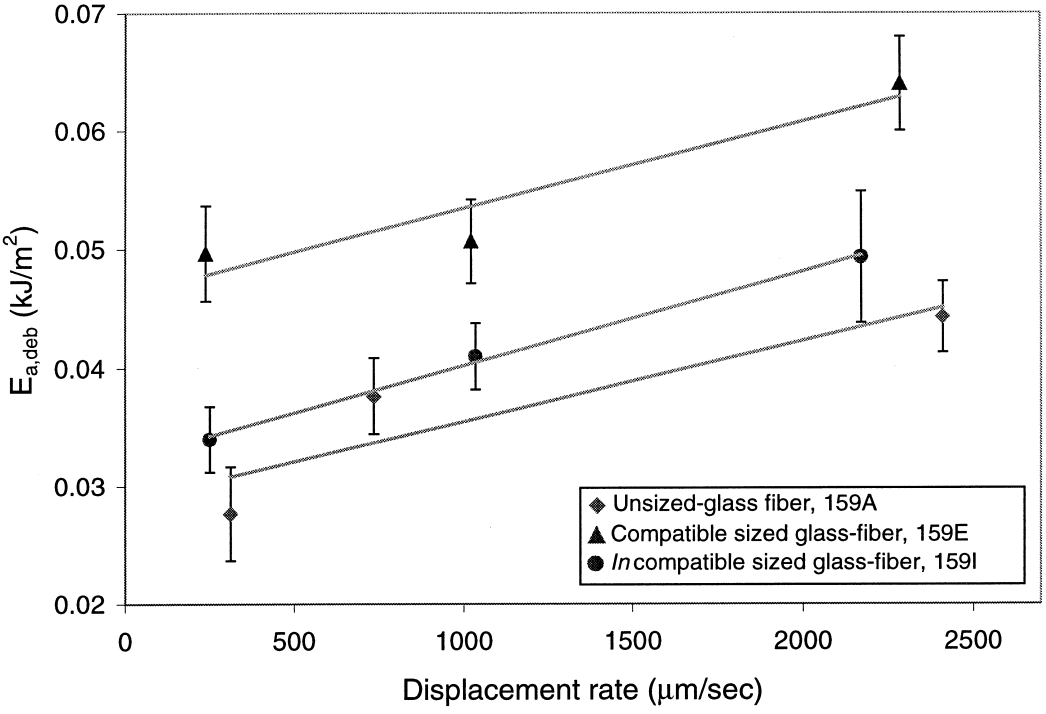

Fig. 8. Energy absorbed within the interphase due to debonding as a function of displacement rate for various sized E-glass-fiber/epoxy-amine interphases.

μm/s) for both unsized and sized systems. The epoxy-amine compatible sized fiber (159E) system showed the highest debonding energy (0.049 kJ/m^2 at 238 μm/s) while the unsized 159A fibers exhibited the lowest (0.027 kJ/m^2 at 312 μm/s). The higher debonding energy of the compatible sizing was attributed to superior interphase adhesion. Moreover, the sized systems failed at displacement values larger than the unsized system, resulting in

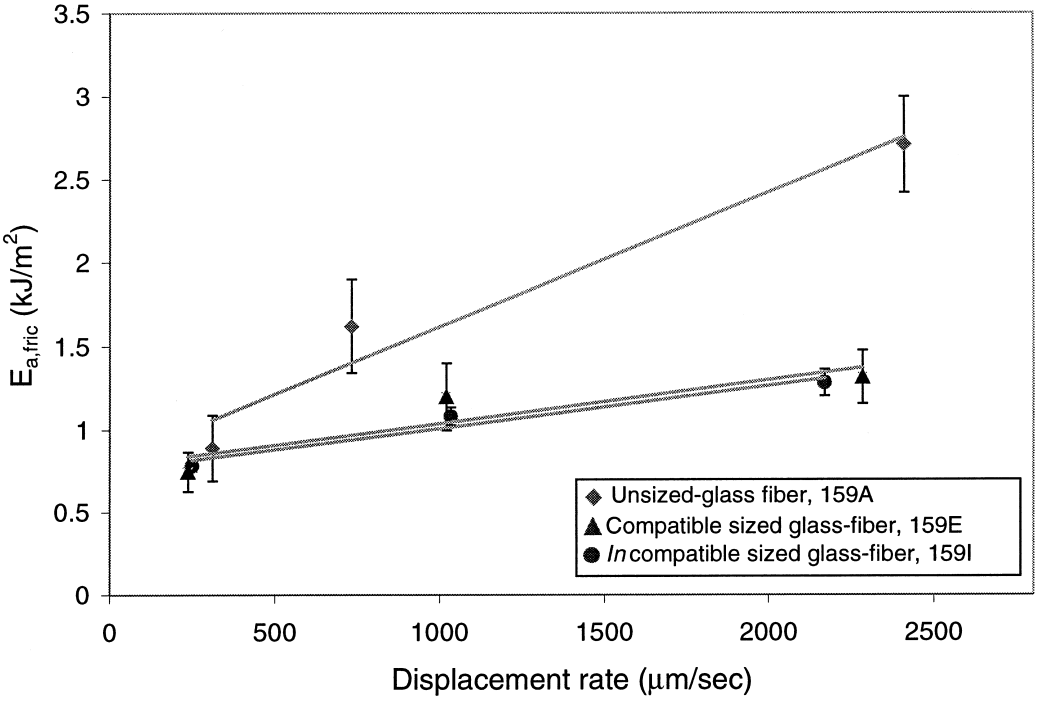

Fig. 9. Energy absorbed within the interphase due to fiber/matrix frictional sliding as a function of displacement rate for various sized E-glass-fiber/epoxy-amine interphases.

higher debonding energy. The debonding energies were also found to be sensitive to the loading rate as seen in Fig. 8. These energies increased almost linearly as the displacement rate increased (38, 23 and 30% increase for 159A, 159E and 159I fiber systems, respectively, in the measured range of displacement rates).

In contrast to the debonding energy, the unsized (159A) system showed higher frictional energy absorption than the sized 159E and 159I fibers, especially at high loading rates. The frictional energy values were also found to be extremely sensitive to the loading rate. In general, for all fiber systems, the frictional energy increased as the loading rate increased. The sized 159E and 159I fiber systems showed almost equal increases as a function of displacement rate. The frictional energies increased about 50% in the range of 230–2450 μm/s displacement rates for sized 159E and 159I systems. However, this increase for the unsized 159A system was more significant, with a 350% increase in frictional energy over a similar range of displacement rates. The higher frictional energy $(E_{a,fric})$ and the higher frictional sliding stress of composite specimens made with unsized 159A fibers was attributed to the higher coefficient of friction between the debonded surfaces in this system.

Once the fiber is debonded from the matrix, the applied shear stresses at the debonded surfaces have to overcome the frictional sliding stresses in order for the fiber sliding to proceed. The frictional sliding stress (τ_f) is the product of the coefficient of the friction (μ) and the radial compressive stresses, i.e. the radial clamping stress (σ_c) and the stress due to the Poisson's expansion of the fiber (σ_p) as shown in Eq. (6) [27–29].

$$\tau_f = -\mu\ (\sigma_c + \sigma_p) \tag{6}$$

The properties of the interphase may affect the value of μ. As mentioned earlier, a siloxane layer forms on sized fiber surfaces from the silane coupling agent that is chemically bound to inorganic glass. The presence of the sizings applied to the fiber may reduce the roughness of the fiber surface by filling the micro-cavities (flaws) on the surface with sizing components. Therefore, for sized systems, the debonded fiber surface may have lower μ and, therefore, lower frictional sliding energies. This hypothesis is supported by research reported in the literature.

Based on the data from Zinck et al. [30], the size of the surface defects on an unsized E-glass fiber (18.1 μm diameter) is in the range of 0.5–0.05 μm. The size of the defects is reduced to below 0.1 μm by treating the glass fiber surface with a silane coupling agent (A1100, γ-aminopropyltriethoxysilane) or a commercial sizing (including A1100 silane, epoxy film former, lubricant, etc.). It was also shown by Zinck et al. [30] that these surface treatments and, therefore, the formation of the siloxane layer fill the flaws or cracks on the surface. Therefore, these layers may reduce the completely debonded fiber/matrix surface roughness. As shown by Kerans et al. [31] translation of initially mating rough interfaces results in a radial displacement between the

fiber and the matrix surface and therefore a radial compressive stress at the interphase. The magnitude of these radial stresses is related to the amplitude of the surface roughness. Since it is expected that application of the sizing reduces the amplitude of the surface roughness, lower roughness induced radial stress and therefore the lower frictional sliding energies can be expected from the sized systems.

The radial clamping stress, which also affects the frictional stresses, may arise from the difference of thermal expansion coefficient of the fiber, the matrix and the interphase as well as from shrinkage of the matrix during cure [27–29]. Therefore, it is reasonable to expect that the properties (stiffness, thickness, etc.) of the interphase formed in various sized composite systems affect the clamping stress and therefore the frictional energies of the system. The effects of the interphase properties on radial thermal residual stresses were predicted based on the stress analysis developed by Skourlis [32], including thermal stresses in a radial direction at the interphase region (the fiber, the matrix and the interphase are structured as three concentric cylinders). However, our predictions using his model showed [19] that the change of the interphase properties does not significantly affect the magnitude of residual stresses for the composite system studied in this work (i.e. about 3% decrease of radial compressive stresses at the interphase by lowering the interphase stiffness by a fraction of 50). Consequently, this does not appear to be a significant mechanism for energy absorption during frictional sliding in these systems.

3.4. Deformation modes of micro-debonding specimen

The specimens tested with DILA were inspected under scanning electron microscope (SEM) to identify the modes of deformation and the micro-debonding processes. Fig. 10 shows an SEM image obtained from the top surface of the unsized 159A glass/epoxy-amine system tested using DILA. As seen in this figure, the debonded fiber was pushed out from the surrounding matrix. The cavity region at the center of the fiber surface is the indentation cavity formed due to the indenter tip/fiber contact. Fig. 11 also shows the back surface of DILA-tested samples made with unsized 159A fiber. As seen from these SEM micrographs, the fiber protrudes from the plane of the back surface. The bottom edges of the protruded fibers fractured during the micro-debonding processes. This is possibly due to the existence of microcracks that formed near the fiber surface during the polishing stages due to the differences in hardness of the glass and epoxy. The smooth surface of the protruded fibers seems to indicate the interfacial detachment of the interphase and the fiber surface. This type of failure mode is reasonable to expect because the shear stress values are the highest near the fiber surface, and their magnitude decays toward the matrix region. However, these observations of the protruded fiber surface are insufficient to definitely conclude whether the failure mode is an interfacial detachment or cohesive failure within the interphase. The expected interphase thickness from the composite systems tested in this study is about 10 nm [19]. A cohesive failure of the interphase may not be distinguishable under these magnifications. Techniques to measure surface characteristics directly on the fiber need to be developed and are the subject of future work.

Tailoring the interphase zone can optimize the strength and energy absorbing capability of impact/ballistic-resistant composite materials (such as armor) [33–36]. In the literature, there is no general consensus on which mechanisms absorb the most energy. There are a large number of variables involved in the energy absorption process, and quantitative data are rather limited. In the next section, we have estimated the significance of the interphase related damage mechanism on the energy absorption in composite armor by using experimental data obtained in this work.

3.5. Energy absorption in composite armor subjected to ballistic impact: a case study

A case study based on a typical glass/epoxy composite subjected to ballistic impact was performed to determine the significance of the interphase-related micro damage modes in absorbing the impact energy. DILA measured specific energy values reported in this paper were used as input in this case study. In summary, ballistic test results were conducted on a 7-psf S2-glass/SC-4 epoxy armor panel manufactured using the Vacuum Assisted Resin Transfer Molding (VARTM) technique [37]. The S2 glass fibers were supplied from Owens Corning Corporation with an epoxy-amine compatible sizing (OCF 463). The velocity (V_p) and the mass m_p of

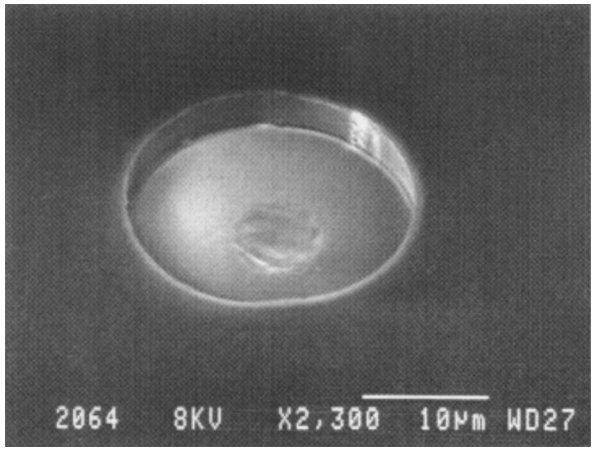

Fig. 10. SEM micrographs (45° tilted) showing the top surface of 159A glass-fiber/epoxy-amine sample tested using DILA.

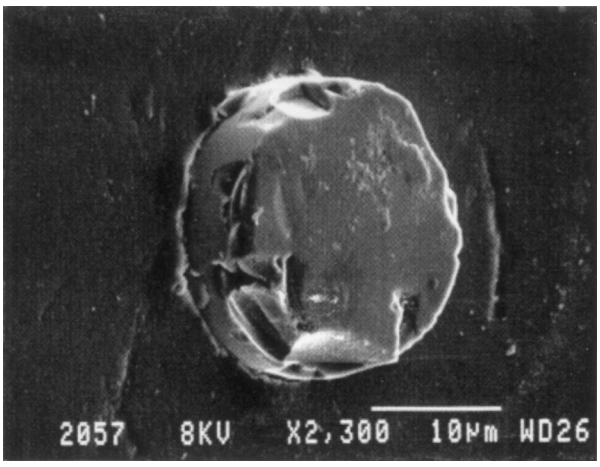

Fig. 11. SEM micrographs showing the back surface of 159A E-glass-fiber/epoxy-amine sample tested using DILA.

the projectile (50 cal FSP) used for impact were 472 mps and 40 g, respectively. The incident kinetic energy of the projectile (E_k) was calculated as follows:

$$E_k = \frac{1}{2} m_p (V_p)^2 \tag{7}$$

A conical damage zone was observed within the armor panel due to the impact. Fig. 12 illustrates the damage zones and the damage modes considered in this case study. The kinetic energy of the projectile can be absorbed by numerous mechanisms including projectile deformation and fracture and macro/micro-mechanical damage in the composite armor. Microscopic observations of the projectile did not reveal any plastic deformation so it is assumed to be a negligible source of energy absorption.

Macro damage considered in this case study focuses on delamination. A sequence of micromechanical damage may occur during stress wave propagation under an impact event or during quasi-static loading [38]. Fig. 13 illustrates the damage sequence where a fiber fails in tension, debonds and pulls out. The debonding of the fiber/matrix interface may initiate due to stress concentration at the free ends of the broken fiber and progress due to the shear and tensile forces at the interface. Once debonding is complete, pull-out of the fiber from the matrix may occur under further loading. The pull-out process is associated with frictional sliding because contact is maintained between the fully debonded fiber and the surrounding matrix. In this case study, energy absorbed due to the micromechanical damages — fragmentation of the fibers (E_{fra}), debonding of the fiber/matrix interphase (E_{deb}), and fiber frictional sliding E_{fric} — was taken into consideration as shown in Eq. (8).

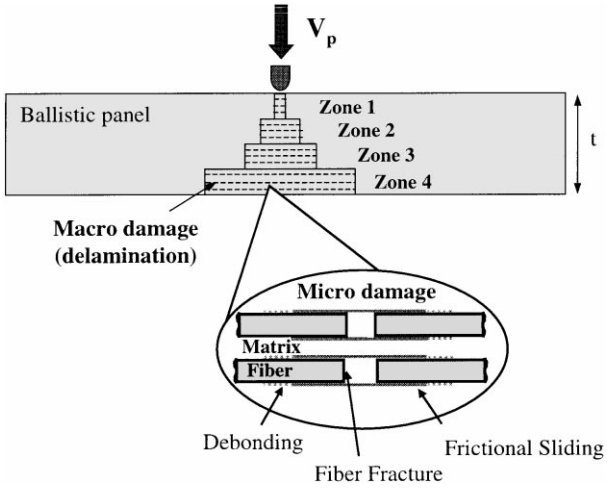

Fig. 12. Schematic illustration of the composite ballistic panel and damage modes (macro and micro) occurred due to ballistic impact.

$$E_k = E_{del} + E_{deb} + E_{fric} + E_{fra} \tag{8}$$

The energy absorbed due to delamination (E_{del}) was calculated using delamination toughness $\left(G_{c,del}\right)$ and the total delamination area $\left(A_{del}^{tot}\right)$ measured using the ultrasonic c-scan technique.

$$E_{del} = A_{del}^{tot} G_{c,del} \tag{9}$$

$$A_{del}^{tot} = \sum_{1}^{n} A_{del,i} \tag{10}$$

where n is the number of plies and A_{del} is the delamination area in each ply. The energies E_{deb} and E_{fric} were calculated from Eqs. (11)–(15). The specific absorbed energies due to debonding $\left(E_{a,deb}\right)$ and frictional sliding $\left(E_{a,fric}\right)$ were obtained from DILA experiments.

$$E_{deb} = A_{deb} E_{a,deb} \tag{11}$$

$$A_{deb} = \frac{2 V_{damage} V_f V_{f,inv}}{r_f} \tag{12}$$

$$E_{fric} = A_{fric} E_{a,fric} \tag{13}$$

$$A_{fric} = 2\pi r_f \frac{l_m}{2} N_{fragment} \tag{14}$$

$$N_{fragment} = \frac{V_{damage} V_f V_{f,inv}}{\pi r_f^2 l_m} \tag{15}$$

where V_{damage} is the volume of material within the conical damage zone measured using ultrasonic. The term V_f is the fiber volume fraction of the composite panel and $V_{f,inv}$ is the fraction of fibers involved that absorb energy by debonding and frictional sliding (the value of

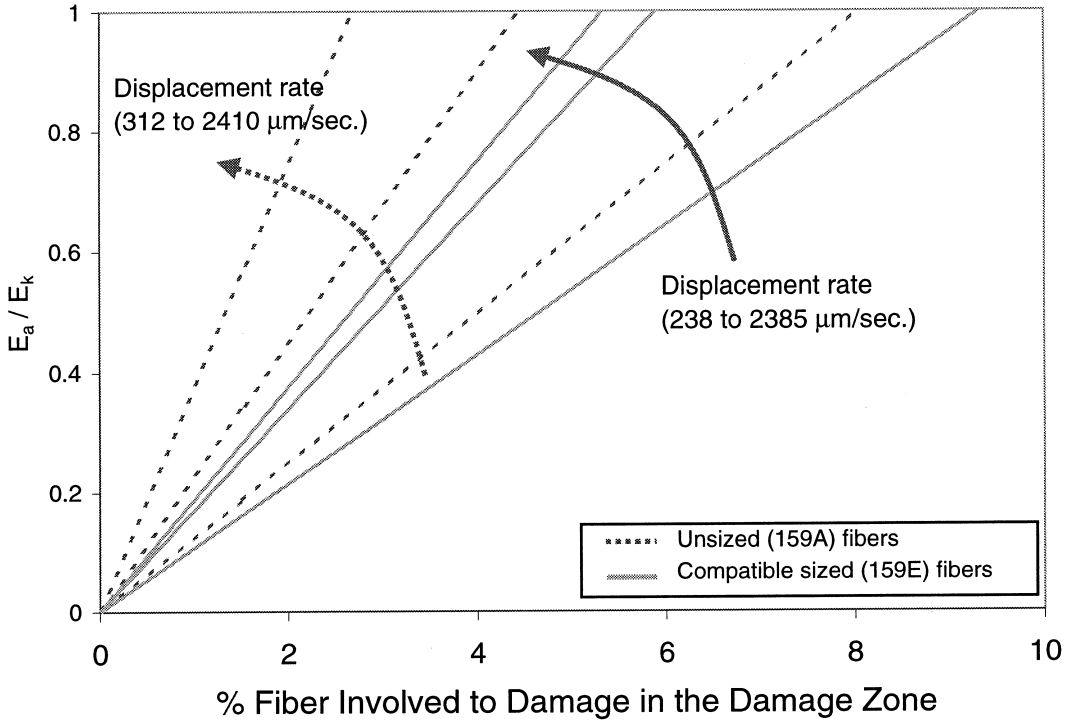

Fig. 13. Total absorbed energy absorbed in fiber/matrix debonding, frictional sliding and fiber fracture normalized by the projectile kinetic energy as a function of% fiber involved to damage in the damage zone. E_a/E_k is shown for unsized 159A fibers and epoxy-amine compatible sized 159E fibers at various loading rates.

$V_{f,inv}$ can not be practically quantified; however, all of the calculated energy is plotted as a function of $V_{f,inv}$ in this study). Also, A_{deb} and A_{fric} are the interfacial areas loaded during debonding and frictional sliding, respectively. The terms l_m and $N_{fragment}$ are the mean fiber fragmentation length and number of fiber fragments. For frictional sliding, it was assumed that the fibers that are involved in the energy-absorbing process slide as much as half of the l_m. This is a reasonable assumption if it is considered that a large amount of deflection occurs during the impact. Moreover, considerable fiber pullout was observed in the impacted panel under the microscope. This may indicate a large amount of frictional sliding distance. The number of fiber fragments $N_{fragment}$ was calculated based on Eq. (14) from the l_m of the glass/epoxy system. The value of l_m was measured using the bimatrix fiber fragmentation technique [19].

The fiber fracture energy (E_{fra}) was calculated mainly from the fiber fracture surface energy (γ_f) and the mean fiber fragmentation length as shown in Eq. (15). It was assumed that the fibers that are involved in damage in the damage zone were transversely fractured in the length of l_m.

$$E_{fra} = 2\pi\ N_{fragment} r_f^2 \gamma_f \tag{16}$$

In the present case study, the energy absorbed due to considered damage mechanisms relative to the kinetic energy of a projectile was calculated based on the inputs summarized in Table 4. Fig. 13 illustrates the total absorbed energy E_a (due to micro damage modes: fiber fracture, fiber/matrix debonding and fiber fracture) normalized by the projectile kinetic energy E_k with respect to the percentage of the fibers involved in the damage zone for compatible sized and sized fibers at various loading rates. For the case examined, the results showed that the interphase-related micro damage modes may absorb a significant fraction of the impact energy even if a relatively small portion (2–5%) of the fibers in the damage zone are damaged in the sequence proposed. Furthermore, the percentage of the fibers required to absorb a certain amount of energy becomes smaller at high loading rates. Fig. 14 shows the energy absorbed due to microscopic damage mechanisms and the delamination relative to the kinetic energy of a projectile as a function of displacement rate for the case of 2% fiber involvement. Since epoxy-amine compatible sized fibers were used in the composite panel examined, it is expected that DILA measured energy values from epoxy-amine compatible sized fiber (159E) systems are most representative for this case study. In order to estimate the effects of the glass fiber sizings on the energy absorbing capability of the fiber/matrix interphase, the energies absorbed within the unsized (159A) and *in*compatible sized (159I) systems are also plotted in Fig. 14. The fiber fracture and delamination energies were assumed insensitive to loading rate. As seen from

Table 4
Data used for energy absorption calculations in the case study

		Date from
Ballistic test data		
Mass of projectile (m_p)	40 (g)	[37]
Velocity of projectile (V_p)	472 (mps)	[37]
Projectile kinetic energy (E_k)	4.45 (kJ)	
Characteristics of the composite panel		
Fiber volume fraction (V_f)	50 (%)	[37]
Number of plies (n)	33	
Dimensions	305×305 (mm×mm)	
Thickness (t)	19 (mm)	
Fiber radius (r_t)	5 (μm)	
Properties		
Delamination fracture toughness $G_{c,del}$	500 (J/m^2)	[39]
Glass fiber surface energy γ_f	5 (J/m^2)	[40]
Mean fiber fragment length (l_m)	652 (μm)	[19]
Delamination area (A_{del}) (From ultrasonic c-scan)		[37]
Zone (gate) location:		
1	0.0022 (m^2)	
2	0.0130 (m^2)	
3	0.0383 (m^2)	
4	0.1227 (m^2)	
Total	0.1765 (m^2)	

Fig. 14, the energy absorbed due to the fiber fracture is negligible. The debonding energies for all the cases are lower than the delamination and frictional sliding. The results revealed that the frictional sliding mechanism would absorb a significantly greater fraction of the energy than debonding, fiber fracture and delamination. Compared to compatible sized 159E and *in*compatible sized 159I fiber systems, the glass/epoxy composite that was made with unsized 159A system may exhibit greater energy-absorbing capability due to the frictional sliding. Moreover, this energy is more sensitive to loading rate compared to that of sized fibers.

The results also indicate that the glass fiber sizing may significantly affect the relative contribution of each energy-absorbing mechanism. Fig. 15 compares the absorbed frictional energy to the strength of unsized 159A and compatible sized 159E systems as a function of displacement rate. As illustrated in this figure an interphase that has lower strength can better contribute to the energy absorption and improve the ballistic performance of a composite armor while an interphase that has higher strength is needed to improve the structural integrity of the composite armor. These results indicate that if micro mechanisms can be triggered during impact loading in the correct sequence, a significant portion of the projectile energy can be absorbed. Therefore, the interphase can be tailored to obtain an

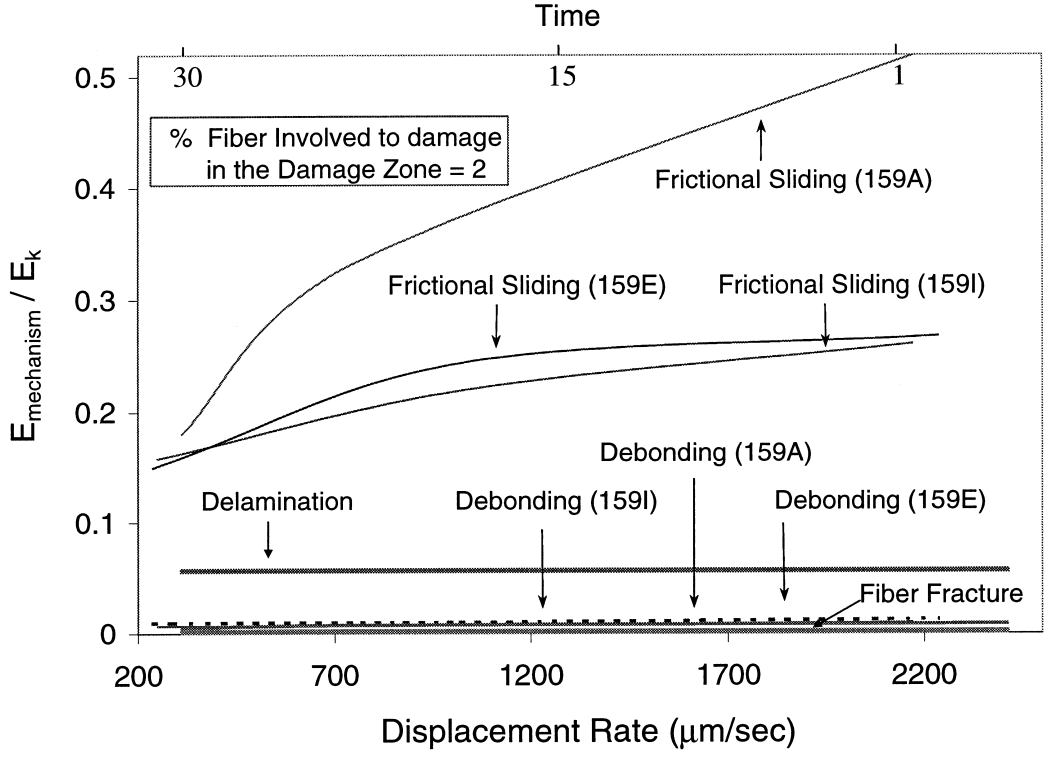

Fig. 14. Absorbed energy due to macro and micro damage modes relative to kinetic energy of the projectile as a function of fiber displacement rate for unsized 159A, compatible sized 159E and incompatible sized 159I fiber systems. $E_{mechanism}$ refers to energy absorbed due to each mechanism shown on the plot.

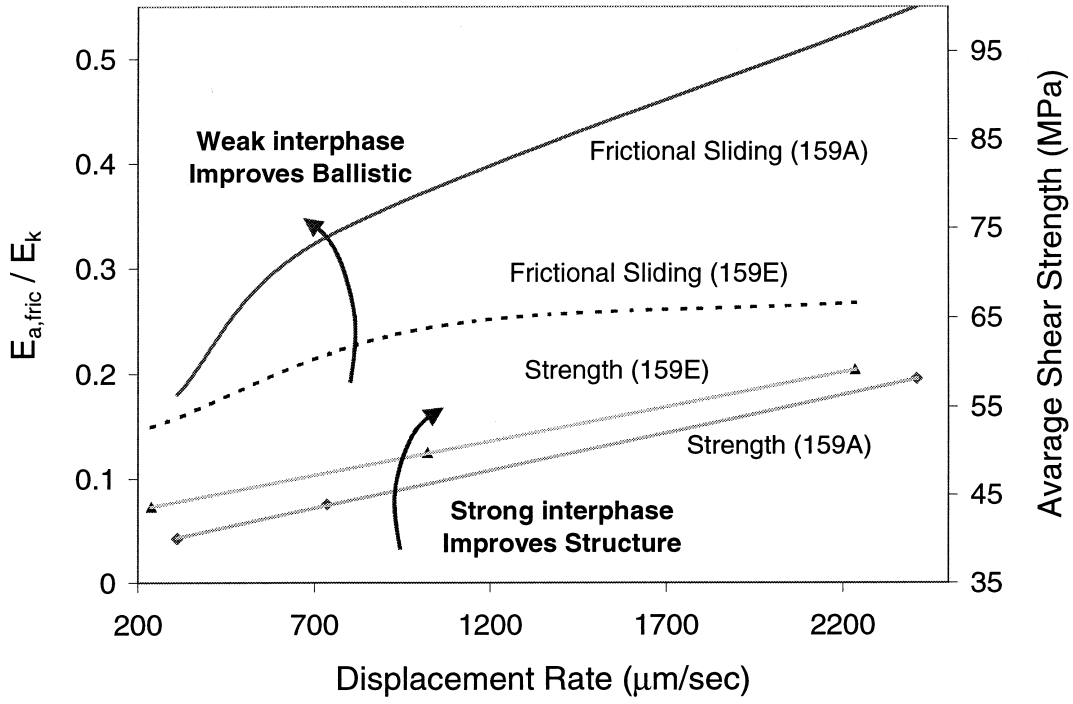

Fig. 15. Comparison of absorbed energy due to fiber/matrix frictional sliding to the average shear strength of fiber/matrix interphase for unsized 159A and compatible sized 159E fiber systems as a function of fiber displacement rate.

optimal balance of energy-absorption and structural performance from the composite.

4. Conclusions

Interphases of various sized E-glass/epoxy-amine systems were tested at displacement rates in the range of 230 to 2450 μm/s using the unique capability of DILA. Interphases that formed due to the presence of various sizings showed significantly different mechanical response. Test results also showed that there is a linear correlation between the interphase shear strength and the loading rate for the range of loading rates studied. In correlating the effects of the fiber sizings on the interphase strength, compatible sizing on the glass fiber increases chemical bonding and adhesion between the inorganic glass and the organic resin phases and strengthens the interphase. The shear strength values increase by about 43, 35 and 27% for composite systems made with unsized 159A, compatible sized 159E, and *in*compatible sized 159I fibers, respectively, over the wide range of displacement rates studied. It was found that a significantly higher amount of energy could be absorbed within the frictional sliding mechanism compared to the debonding mechanism. Moreover, the absorbed energy due to frictional sliding was higher for the interphase that formed in the presence of the unsized 159A fibers. This was attributed to the higher frictional stresses that were developed due to the higher fiber surface roughness. The ability of the interphase to absorb energy was also found to increase with increasing loading rate. The frictional energy increased by about 50% in the case of the model composite systems made with compatible sized 159E and *in*compatible sized 159I fibers, and by 350% in the case of unsized 159A fibers over the range of displacement rates studied. In summary, these results showed that the energy absorbing capability and the shear strength of the fiber/matrix interphase is affected by the properties of the interphase and the loading rate. The case study performed on S2-glass/SC-4 epoxy system showed that interphase related micro damage modes can absorb a significant amount of the impact energy even if a small percentage (2–5%) of the fibers is involved within the damage zone. The frictional sliding can be a significant contributor to energy absorption if this mechanism can be triggered under impact conditions. In summary, an interphase that has lower strength may better contribute to energy absorption, while an interphase with higher strength is needed for structural integrity and environmental durability. Therefore, optimum ballistic and structural performance from the composite can be obtained by tailoring the interphase.

Acknowledgements

The authors gratefully acknowledge the support of the US Army Research Laboratory (ARL) under the

Composite Materials Research Collaborative Program (CMRCP) and the Defense University Research Instrumentation Program (DURIP). The authors also acknowledge Dr. L. Adzima of Owens Corning Corporation for providing the glass fibers.

References

[1] Drzal LT. Composite property dependence on the fiber, matrix and interphase. In: Tough composite materials, Noyes; Park Ridge, 1985. p. 207–22.
[2] Williams JG, James MR, Morris WL. Formation of the interphase in organic-matrix composites. Composites 1994;25:757–62.
[3] Palmese GR, McCullough RL, Sottos NR. J Adhesion 1995;52:101–13.
[4] Piggot MR. In: Vigo TL, Kinzig BJ. editors. Composite applications, the role of matrix, fiber and interface. VCH Publishers, Inc., 1992.
[5] Palmese G.R. Origin and influence of interphase material property gradients in thermosetting composites. PhD. dissertation, University of Delaware, Newark, DE, 1992.
[6] Thomason JL. The interface region in glass fiber-reinforced epoxy resin composites: 3. Characterization of fiber surface coatings and the interphase. Composites 1995;26:487–98.
[7] Drown EK, Al Moussawi H, Drzal LT. Glass fiber sizings and their role in fiber-matrix adhesion. J Adhesion Science and Technology 1991;5:865–81.
[8] Berg J, Jones FR. The role of sizing resins, coupling agents and their blends on the formation of the interphase in glass fiber composites. Composites 1998;Part A:1261–72.
[9] Mader E, Grundke K, Jacobasch H-J, Wachinger G. Surface, interphase and composite relations in fiber-reinforced composites. Composites 1994;25:739–44.
[10] Hoecker F, Karger-Kocsis J. Effects of the interface on the mechanical response of CF/EP microcomposites and macrocomposites. Composites 1994;25:729–38.
[11] Subramanian S, Lesko JJ, Reifsnider KL, Stinchcomb KL. Characterization of the fiber-matrix interphase and its influence on mechanical properties of unidirectional composites. J of Composite Materials 1996;30:309–32.
[12] Hartman DR. Ballistic materials. US Patent, 4,842,923, 27 June 1989.
[13] Agbossou A, Cohen I, Muller D. Effects of interphase and impact strain rates on tensile off-axis behavior of unidirectional glass fibre composite: experimental results. Engineering Fracture Mechanics 1995;52:923–34.
[14] Kim J-K, Mai Y-W. Engineered interfaces in fiber reinforced composites. Oxford: Elsevier Science, 1998.
[15] Lauke B, Schultric B, Barthel R. Contribution to the micromechanical interpretation of fracture work of short-fiber reinforced thermoplastics. Compos Sci and Technol 1985;23:21–35.
[16] Gupta VB, Mittal RK, Goel M. Energy absorbing mechanisms in short-glass-fiber reinforced polypropylene. Compos Sci and Technol 1990;37:353–69.
[17] Bandyopadhyay S, Gellert EP, Silva VM, Underwood JH. Microscopic aspects of failure and fracture in cross-ply fiber reinforced composite laminates. J Composite Materials 1989;23:1217–31.
[18] Cantwell WJ, Morton J. The impact resistance of composite materials-a review. Composites 1991;22:347–62.
[19] Tanoglu M. Investigation of the fiber/matrix interphase under high loading rates. PhD. dissertation, University of Delaware, Newark, DE, 2000.
[20] Tanoglu M, Ziaee S, McKnight SH, Gillespie Jr JW, Palmese GR. Investigation of properties of the interphase formed due to the glass fiber sizings. Submitted to J. of Materials Science, December 1999.
[21] Tanoglu S, McKnight SH, Palmese GR, Gillespie Jr. J.W. A new technique to characterize the fiber/matrix interphase properties under high-strain-rates. Submitted to Composites, Part A, August 1999.
[22] Kallas MN, Koss DA, Hahn HT, Hellmann JR. Interfacial stress state present in a thin-slice; fibre push-out test. J of Materials Science 1992;27:3821–6.
[23] Mandell JF, Grande DH, Tsiang T, McGarry FJ. Modified microdebonding test for direct in situ fiber/matrix bond strength determination in fiber composites. In: Whitney JM, editor. In: Composite materials: testing and design (seventh conference). Philadelphia: ASTM STP 893, 1986. p. 87–108.
[24] Bechel VT, Sottos NR. Application of debond length measurements to examine the mechanics of fiber pushout. J Mech Phys Solids 1998;46:1675–97.
[25] Bechel VT, Sottos NR. The effect of residual stresses and sample preparation on progressive debonding during the fiber push-out test. Compos Sci and Technol 1998;58:1741–51.
[26] Netravali AN, Stone D, Ruoff S, Topoleski LTT. Continuous micro-indenter push-through technique for measuring interfacial shear strength of fiber composites. Compos Sci Technol 1989;34:289–303.
[27] Hsueh CH. Interfacial friction analysis for fibre-reinforced composites during fibre push-down (indentation). J Materials Science 1990;25:818–28.
[28] Chen EJH, Croman RB. Microdebonding investigation of the effects of thermal residual stress on the bond strength of a graphite/polyamide composite. Compos Sci and Technol 1993;48:173–9.
[29] Mukherjee S, Ananth CR, Chandra N. Effects of residual stresses on the interfacial fracture behavior of metal-matrix composites. Compos Sci and Technol 1997;57:1501–12.
[30] Zinck P, Pays MF, Rezakhanlou R, Gerards JF. Mechanical characterization of glass fibres as an indirect analysis of the effect of surface treatment. J of Materials Science 1999;34:2121–33.
[31] Kerans RJ, Parthasarathy TA. Theoretical analysis of the fiber pullout and pushout test. J Am Ceram Soc 1991;74:1585–96.
[32] Skourlis TP. Structure and properties of the interphase in coated carbon-fiber/epoxy systems. PhD dissertation, University of Delaware, Newark, DE, 1995.
[33] Madhukar MS, Drzal L. Fiber-matrix adhesion and its effect on composite mechanical properties: IV. Mode I and Mode II fracture toughness of graphite/epoxy composites. J Composite Materials 1992;26:936–68.
[34] Labronici M, Ishida H. Toughening composites by fiber coating: a review. Composite Interfaces 1994;2:199–234.
[35] Rydin RW, Karbhari VM. Glass fabric vinyl-ester composites: Tailoring the fiber bundle/matrix interphase with nylon coatings to modify energy absorption behavior. J Composite Materials 1997;31:183–209.
[36] Smith Jr WN. Lightweight armor. US Patent, 4,732,803, Mar. 22, 1988.
[37] Fink BK, Bernetich KR, Gillespie Jr. JW. US Army Research Laboratory Report, Aberdeen Proving Ground, MA, in press.
[38] Beaumont PWR, Schultz JM. Micromechanisms of fracture in continuous fiber composites — Part 1: theory. In Delaware composites design encyclopedia, vol. 4. Technomic Publishing Company, 1990.
[39] Monib AM. Damage tolerance of thick-section composites subjected to ballistic impact. Master thesis, University of Delaware, Newark, DE, 1999.
[40] Wagner HD, Lustiger A. Effect of water on the mechanical adhesion of the glass/epoxy interface. Composites 1994;25:613–6.